The Structures of Human Dihydroorotate Dehydrogenase with and without Inhibitor Reveal Conformational Flexibility in the Inhibitor and Substrate Binding Sites[†]

Björn Walse,*[,‡] Veronica Tamu Dufe,[§,||] Bo Svensson,[‡] Ingela Fritzson,[⊥] Leif Dahlberg,[⊥] Alfia Khairoullina,[⊥] Ulf Wellmar,[⊥] and Salam Al-Karadaghi*[,§]

SARomics AB, P.O. Box 724, SE-220 07 Lund, Sweden, Department of Molecular Biophysics, Center for Molecular Protein Science, Lund University, Box 124, SE-221 00 Lund, Sweden, and Active Biotech Research AB, P.O. Box 724, SE-220 07 Lund, Sweden

Received February 27, 2008; Revised Manuscript Received June 25, 2008

ABSTRACT: Inhibitors of dihydroorotate dehydrogenase (DHODH) have been suggested for the treatment of rheumatoid arthritis, psoriasis, autoimmune diseases, *Plasmodium,* and bacterial and fungal infections. Here we present the structures of N-terminally truncated (residues Met30−Arg396) DHODH in complex with two inhibitors: a brequinar analogue (**6**) and a novel inhibitor (a fenamic acid derivative) (**7**), as well as the first structure of the enzyme to be characterized without any bound inhibitor. It is shown that **7** uses the "standard" brequinar binding mode and, in addition, interacts with Tyr356, a residue conserved in most class 2 DHODH proteins. Compared to the inhibitor-free structure, some of the amino acid side chains in the tunnel in which brequinar binds and which was suggested to be the binding site of ubiquinone undergo changes in conformation upon inhibitor binding. Using our data, the loop regions of residues Leu68−Arg72 and Asn212−Leu224, which were disordered in previously studied human DHODH structures, could be built into the electron density. The first of these loops, which is located at the entrance to the inhibitor-binding pocket, shows different conformations in the three structures, suggesting that it may interfere with inhibitor/cofactor binding. The second loop has been suggested to control the access of dihydroorotate to the active site of the enzyme and may be an important player in the enzymatic reaction. These observations provide new insights into the dynamic features of the DHODH reaction and suggest new approaches to the design of inhibitors against DHODH.

Dihydroorotate dehydrogenase (DHODH,[1] EC 1.3.99.11) is a key enzyme in nucleotide synthesis. It catalyzes the fourth committed step in the de novo biosynthesis of pyrimidines. In this step of the synthesis, (*S*)-dihydroorotate (DHO) is stereospecifically oxidized to orotate, while the prosthetic flavin (FMN) group is reduced. Inhibition of DHODH leads to reduced levels of essential pyrimidine precursors, among which is UMP, a critical component of RNA and DNA synthesis (*1*). Most organisms are able to both synthesize and salvage pyrimidine bases; however, rapidly proliferating human cells such as activated T-lymphocytes (*2*) and cancer cells (*3*) are dependent on de novo nucleotide synthesis to meet their growth requirements (*1*). The suggestion that DHODH inhibitors may be used as antiproliferative agents in cancer therapy and to treat tropical parasitic infections is based on these findings (*4–9*). Brequinar and leflunomide are two examples of such compounds that have been clinically tested. Brequinar (denoted **1** in Table 1) is an antitumor and immunosuppressive agent, while leflunomide, which is a prodrug to the active metabolite A771726 (denoted **2** in Table 1), shows immunosuppressive activity (*6, 10–16*). Unfortunately, oral administration of brequinar together with cyclosporine or cisplatin has been shown to have toxic effects such as mucositis, leukocytopenia, and thrombocytopenia (*10, 17, 18*). Severe side effects like diarrhea, abnormalities in liver enzymes, rash, and hypertension have also been observed during clinical use of lefluonomide (Arava) (*19–23*). Thus, there is still a need for new and more efficient DHODH inhibitors with reduced side effects.

DHODH proteins from different organisms have been grouped into two classes. The first class (class 1) includes the cytosolic family, while the second class (class 2) includes membrane-associated DHODH (*24*). Class 2, to which human DHODH belongs, is distinguished from class 1 by the use of ubiquinone for reoxidizing FMN and by the presence of a highly variable N-terminal extension, which is responsible for the association of the enzyme with the inner mitochondrial membrane (*24, 25*). The N-terminal extension

[†] This work has been supported by a grant from the Graduate School of Pharmaceutical Sciences at Lund University (FLÄK) to S.A.-K.

* To whom correspondence should be addressed. S.A.-K.: Department of Molecular Biophysics, Center for Molecular Protein Science, Lund University, P.O. Box 124, SE-221 00 Lund, Sweden; telephone, +46 46 222 4512; fax, +46 46 222 4692; e-mail, salam.al-karadaghi@mbfys.lu.se. B.W.: SARomics AB, P.O. Box 724, SE-220 07 Lund, Sweden; telephone, +46 46 19 1276; fax, +46 46 19 1277; e-mail, bjorn.walse@saromics.com.

[‡] SARomics AB.

[§] Lund University.

[||] Present address: Institute of Biochemistry, University of Luebeck Ratzeburger Allee 160, 23538 Luebeck, Germany.

[⊥] Active Biotech Research AB.

[1] Abbreviations: DHODH, dihydroorotate dehydrogenase; C_{11}DAO, *N*,*N*-dimethylundecylamine *N*-oxide; DDAO, *N*,*N*-dimethyldodecylamine *N*-oxide; DMSO, dimethyl sulfoxide; DCIP, dichloroindophenol; rmsd, root-mean-square deviation.

10.1021/bi8003318 CCC: $40.75
Published on Web 08/02/2008

Table 1: Molecular Structures and IC_{50} Values for Some Inhibitors of Human DHODH (**6**, **7**, and **8** used in this study)[a]

Code	Chemical Structure	IC_{50}
1	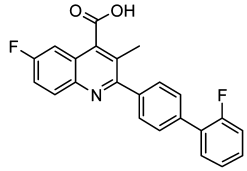	6 nM, (*33*)
2	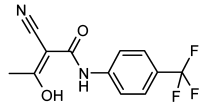	773 μM, (*33*)
3	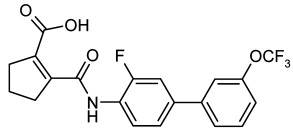	280 nM, (*28*)
4	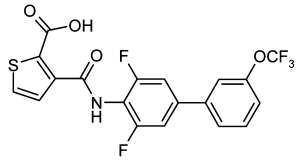	2 nM, (*28*)
5	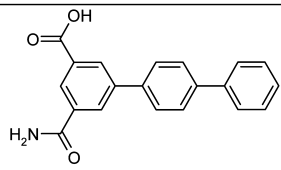	K_i 2.8 μM, (*34*)
6	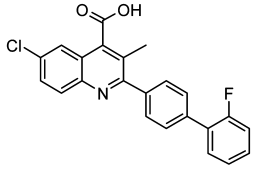	15 nM[a]
7	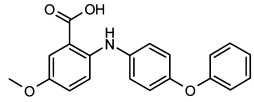	81 nM[a]
8	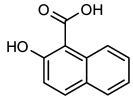	63 μM[a]

[a] The IC_{50} values were determined by the standard DCIP assay using saturated concentrations of DHO (200 μM) and decylubiquinone (CoQd) (*41*).

folds into a separate domain with two α-helices (Figure 1). It is located on top of the catalytic C-terminal domain close to the FMN binding site and contributes to the formation of a tunnel-like pocket (*7, 26, 27*). Some inhibitors of class 2 DHODH have been found to bind inside this tunnel, which has led to the suggestion that ubiquinone may also bind there (*7, 26, 28–33*). The C-terminal domain is folded into an α/β barrel, and in addition to the FMN binding site, it contains the active site where dihydroorotate binds.

The crystal structures of human DHODH in complex with a brequinar analogue 2′-desfluorobrequinar, with A771726 (an active metabolite of leflunomide, **2** in Table 1), and in complex with a series of novel compounds with binding modes described as being brequinar-like, nonbrequinar-like, or dual (e.g., compounds **3** and **4** in Table 1) have been

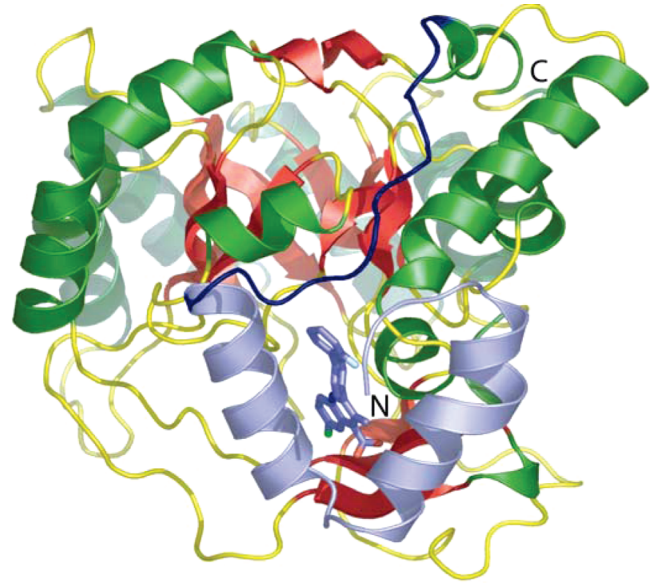

FIGURE 1: Overall view of the structure of human DHODH in complex with compound **7**. The helices of the N-terminal helical domain are colored light blue, and the bound inhibitor is shown as sticks. The loop connecting the N- and C-terminal domains is colored dark blue. In the core catalytic domain, helices are colored green, strands red, and loop regions yellow. The figures were prepared with Pymol (*50*).

determined (*7, 28*). Compounds with a brequinar-like binding mode had lower IC_{50} values, indicating a higher binding affinity. In addition, the crystal structure of a terphenyl inhibitor (**5** in Table 1) designed to be a hybrid between the scaffold of **1** and the binding motif of **2** has been reported (*34*). Here we present the first crystal structure of the inhibitor-free N-terminally truncated (residues Met30−Arg396) human DHODH, as well as the structures of two complexes, one with a brequinar analogue (**6**) and the other with a novel inhibitor (**7**) with a different chemotype as compared to the previously known inhibitors.

EXPERIMENTAL PROCEDURES

Cloning, Expression, and Purification of Human DHODH. The RNA encoding N-terminally truncated human DHODH (Met30−Arg396) was isolated from U937 cells using the All Perfect RNA Mini Kit (QIAGEN) and amplified by RT-PCR (Titan one-tube RT-PCT system, Roche) using the upstream primer 5′-TTCAGCTACATATGGCCACGG-GAGATGAGCGTTTC-3′ (35-mer with the endonuclease *Nde*I restriction site underlined) and the downstream primer 5′-CATTCGTAGGATCCTCACCTCCGATGATCTGCTCC-3′ (35-mer with the *Bam*HI site underlined). The PCR product was digested with *Nde*I and *Bam*HI and cloned into the pET-19b expression vector (Novagen) according to standard procedures outlined in the Novagen PET system manual. The entire coding region was confirmed by DNA sequencing. The vector produces DHODH as a fusion protein with 10 N-terminal His residues. To produce the protein, the plasmid was used to transform competent BL21(DE3) cells (Novagen). These bacteria, BL21(DE3)/DHODH, from a frozen stock were precultured at 25 °C in 2× YT medium using ampicillin as a selection marker. The preculture was used to inoculate a 5 L fermentor, from which the cells were harvested after being cultivated for 19 h without any addition

of inducer. Part of the frozen cell pellet (33.2 g) was dissolved in 150 mL of cold buffer [50 mM HEPES (pH 7.0), 300 mM NaCl, and 10% glycerol] supplemented with two tablets of Complete Protease Inhibitor Cocktail (Roche). Lysozyme (Merck), 150 μg, was added, and the cell solution was kept in motion for 45 min at 20 °C. After addition of 60 μL of Benzonase (Merck) followed by incubation for an additional 30 min, the cell slurry was sonicated (4 × 20 s) under ice at 30 s intervals. After addition of 1% Triton X-100, the solution was centrifuged at 38000*g* for 1.5 h at 4 °C. The supernatant was applied to a column packed with 5 mL of Talon superflow resin (Clontech), previously equilibrated with the same HEPES buffer described above. After being extensively washed, the proteins were eluted with 300 mM imidazole. The imidazole was later removed from the eluted proteins when they were passed through PD-10 columns (Amersham). The yield of the pure enzyme was approximately 60 mg, and spectral analysis showed the characteristic absorption maxima at 363 and 456 nm originating from the flavin moiety. These decreased in magnitude after the addition of the substrate dihydroorotate. After addition of the electron acceptor decylubiquinone, the absorption maxima could be recorded again, although at a slightly higher wavelength, probably due to the presence of the product orotate. The His_{10} tag was not removed for further studies.

Cocrystallization of DHODH with Inhibitor. Purified DHODH used for crystallization trials was concentrated to more than 20 mg/mL by using Centriprep centrifugal concentrators (Amicon) followed by Microcon centrifugal filter devices (Amicon). The protein at a concentration of 18−24 mg/mL [dissolved in 10 mM *N*,*N*-dimethylundecylamine *N*-oxide (C_{11}DAO) (Fluka), 400 mM NaCl, 1 mM EDTA, 100 mM HEPES (pH 7), and 30% glycerol] was mixed with an equivalent volume of the crystallization buffer, consisting of 100 mM acetate (pH 4.8), 40 mM C_{11}DAO, 20.8 mM *N*,*N*-dimethyldodecylamine *N*-oxide (DDAO) (Fluka), 2 mM dihydroorotic acid (DHO) (Sigma), and varying concentrations of $(NH_4)_2SO_4$ (1.6−2.2 M). Inhibitor compounds dissolved in dimethyl sulfoxide (DMSO) (Eurisotop) were added to the mixture described above (1−10 μL). The resulting protein and inhibitor solution was mixed in equal amounts with the reservoir buffer consisting of 100 mM acetate (pH 4.8), various concentrations of $(NH_4)_2SO_4$ (from 1.6 to 2.2 M), and 30% glycerol. Hanging drops of 5−10 μL were prepared using siliconized circle cover slides (HR3-231, Hampton Research). Streak seeding was done by gently touching an old protein/precipitant drop with a whisker, thereby transferring seeds of small crystals into a new protein/precipitant drop. Crystals usually appeared after a few days and reached full size in approximately 3 weeks.

Data Collection, Structure Determination, and Refinement. All data sets were collected at beamline I711 at the MAX-II synchrotron radiation source in Lund, Sweden (*35*), using a Mar345 image plate detector. Crystals were flash-frozen in liquid nitrogen and kept at 100 K during data collection. The crystals belonged to space group $P3_221$ with the following cell dimensions: $a = b = 90.5$ Å and $c = 122.0$ Å. The data sets were processed using XDS (*36*). The structures of the complexes were determined by molecular replacement using CNS (*37*) with the DHODH−brequinar analogue complex [Protein Data Bank (PDB) entry 1d3g (*7*)] as the starting model. Model building and refinement were conducted with O (*38*) and CNS. At later stages of refinement, Refmac 5.0.2 was used (*39*). Details of data collection and refinement statistics are presented in Table 2. The coordinates of the complexes (compounds **6** and **7**) and the apo structure have been deposited in the Protein Data Bank as entries 2PRH, 2PRL, and 2PRM, respectively.

Synthesis of Compounds. (i) Compound **6.** 6-Chloro-2-(2′-fluorobiphenyl-4-yl)-3-methylquinoline-4-carboxylic acid (6-chloro brequinar), a brequinar analogue, was prepared by the Pfitzinger condensation of 5-chloroisatin and the 4-propionylbiphenyl (*40*). The following analytical NMR data were obtained for this compound: ^{1}H NMR (500 MHz, DMSO) δ 2.44 (3H, s), 7.32−7.37 (2H, m), 7.43−7.48 (1H, m), 7.63 (1H, dt), 7.70 (2H, d), 7.74 (2H, d), 7.78−7.82 (2H, m), 8.07 (1H, d), 14.5 (1H, bs); MS *m*/*z* 392 $(M + H)^+$.

(ii) Compound **7.** 5-Methoxy-2-(4-phenoxyphenylamino)benzoic acid, 2-bromo-5-methoxybenzoic acid (14.8 g, 64 mmol), and 4-phenoxyaniline (23.7 g, 128 mmol) were dissolved in 50 mL of DMF. Potassium carbonate (4.44 g, 32 mmol) and copper bronze (0.40 g) were added, and the reaction mixture was heated to 150 °C for 2 h. The reaction mixture was allowed to reach room temperature and was then added dropwise to hydrochloric acid (6 M, 200 mL). The resulting precipitate was collected by filtration with suction and washed with water. The crude product was recrystallized from ethanol (150 mL), giving 16.01 g of the title compound (74.6%). The following analytical data were obtained for this compound: ^{1}H NMR (400 MHz, $CDCl_3$) δ 3.73 (3H, s), 6.98 (4H, d), 7.04−7.12 (2H, m), 7.18 (3H, t), 7.32−7.41 (3H, m), 9.15 (1H, s); MS *m*/*z* 336 $(M + H)^+$. Anal. Calcd for $C_{20}H_{17}NO_4$: C, H, 5.11; N, 4.18. Found, C, H, 5.16; N, 4.29.

(iii) Compound **8.** 2-Hydroxy-1-naphthoic acid was purchased from Sigma-Aldrich (catalog no. H45809).

Enzymatic Assay for Inhibition of Recombinant Human DHODH Activity. IC_{50} values for compounds **6**−**8** were determined with the following method. DHODH activity in recombinant N-terminally truncated human DHODH was assayed by DHO-driven reduction of dichloroindophenol (DCIP) (*41*). The recombinant enzyme at a final concentration of 0.4 μg/mL in PBS supplemented with 0.02% Tween 20 was preincubated with or without inhibitor in a buffer containing 50 mM Tris (pH 8), 0.1% Triton X-100, 1 mM KCN, 100 μM decylubiquinone, and 200 μM DCIP for 30 min at room temperature. The reaction was initiated by the addition of 500 μM DHO, and the reduction of DCIP was measured after 10 min as a decrease in absorbance at 650 nM. Absorbance was plotted as a percentage of control at various drug concentrations, and IC_{50} was calculated.

RESULTS

Data were collected from DHODH crystallized in the presence of three different compounds, a brequinar analogue (6-chloro brequinar, in which the 6-fluoro group of brequinar is replaced with a 6-chloro group; compound **6**), a novel inhibitor (compound **7**), and a hydroxynaphthoic acid (2-hydroxy-1-naphthoic acid, compound **8**) (Tables 1 and 2). While the first two inhibitors could be clearly detected in the electron density maps, no electron density for compound **8** was seen, indicating a low binding affinity and a low occupancy of the site (Table 1). This resulted in the first structure of an inhibitor-free enzyme.

Table 2: Data Collection and Refinement Statistics for the Three Structures Presented in This Work

	6	**7**	**8** (inhibitor-free)
cell dimensions[a] *a*, *c* (Å)	90.6, 122.7	90.4, 122.1	90.1, 123.2
resolution range (Å)	20.0−2.3	20.0−2.1	20.0−3.0
completeness (%)	99.7 (100.0)[b]	98.1 (98.4)[b]	99.5 (100.0)[b]
no. of unique reflections	26327	33570	11941
$I/\sigma(I)$	12.0 (4.0)[b]	10.55 (5.9)[b]	6.9 (5.0)[b]
R_{merge} (%)[c]	11.8 (39.6)[b]	11.9 (29.6)[b]	25.0 (34.6)[b]
no. of protein atoms	2805	2805	2805
no. of water molecules	344	196	33
R_{cryst} (R_{free})[d]	0.198 (0.220)[b]	0.185 (0.207)[b]	0.209 (0.253)[b]
average *B*-factor (Å^2)	21.2	20.5	21.6
rmsd for bond lengths (Å)	0.008	0.009	0.009
rmsd for bond angles (deg)	1.4	1.6	1.4
rmsd for dihedrals (deg)	21.4	21.4	21.7

[a] Space group $P3_221$. [b] The numbers in parentheses are for the highest-resolution shell. [c] $R_{merge} = \sum_i |I - \langle I \rangle| / \sum_i (I)$. [d] $R_{cryst} = \sum |F_{obs} - F_{calc}| / \sum F_{obs}$, where F_{obs} and F_{calc} are the observed and calculated structure factor amplitudes, respectively. R_{free} is the same as R_{cryst}, but calculated on 5% of the data excluded from refinement.

Structures of the Complex with Compound **6** *(brequina-Cl−DHODH) and the Inhibitor-Free Enzyme.* Superposition of an earlier structure of a complex with another brequinar analogue (*7*) and the structure of the complex with compound **6** shows identical binding modes for the two molecules in the tunnel formed by the N-terminal domain (Figure 1). An extensive network of interactions (not shown) provides the basis of the high affinity of brequinar analogues for human DHODH [$IC_{50} < 0.01$ μM (Table 1)]. The major difference observed between this structure and the previously published complex with a brequinar analogue is that the region between amino acid residues Leu68 and Arg72, which lacked interpretable electron density in the previous structures, could be built into the electron density map of the complex presented here (Figure 2A). This region belongs to a long loop, which follows helix α2 and connects the N- and C-terminal domains of the molecule (shown in Figure 1). Apart from this, we have also rebuilt the N-terminus, which appears to have a different conformation in our complex, being bent toward the inhibitor-binding pocket. The previously published complex of brequinar with human DHODH showed a detergent molecule associated with the N-terminal region, which partially covered the biphenyl moiety of the inhibitor (*7*). In the complex presented here, some trace density, which may correspond to this detergent molecule, could be seen at the level of 1σ, but not at 1.2σ. There are no traces of the detergent molecule in the structure of the inhibitor-free enzyme, which may be an effect of the lower resolution and/or the absence of the inhibitor (which may stabilize detergent binding).

As noted above, cocrystallization of DHODH with hydroxynaphthoic acid resulted in an inhibitor-free structure of the enzyme. A comparison of the structure of the complex with compound **6** with that of the inhibitor-free enzyme showed several interesting differences. Thus, the loop region between Leu68 and Arg72 has two different conformations in the two structures (Figure 2B). In the inhibitor complex, the side chain of Leu68 moves by approximately 2.5 Å to avoid a steric clash with the biphenyl moiety of the inhibitor. The flexibility of this loop region suggests that it may have a gatekeeping function, controlling binding and dissociation of ubiquinone, which has been suggested to bind in the same tunnel as the brequinar-like inhibitors. In addition, the side chains of several residues, described previously as primary interaction partners with inhibitors (*7, 28, 29*), undergo a conformational change (Figure 3): Met43, Leu46, Gln47, Val134, and Arg136. Although these conformational changes are limited to the side chains, they show the ability of the binding pocket to adapt to the bound molecule, and they should be taken into account when new inhibitors are designed.

An interesting feature of the inhibitor-free structure is that the loop between amino acid residues Asn212 and Leu224, which includes several invariant and conserved residues, is well-resolved in the electron density map (Figure 4). In all previous human DHODH structures, including the complex with compound **6**, this loop was disordered, perhaps due to high flexibility, which led to the conclusion that it may function in controlling the access of dihydroorotate to the active site of the enzyme (*7*). In the inhibitor-free structure, the side chain of Asn217 makes a hydrogen bond (2.6 Å) with the carboxylic group of orotate, apparently contributing to the stability of the substrate in the active site. It is tempting to speculate that the presence of the inhibitor (or the quinone cofactor) may destabilize the conformation of this loop, thus providing a mechanism for orotate release. However, there is no apparent interaction between the inhibitor and any of the loop residues: the distance from the Cl atom of compound **6** to the side chain of Asn217 is approximately 12 Å.

Structure of the Complex with Compound **7.** Apart from redoxal (*42*), compounds from the fenamic acid class (*N*-aryl anthranilic acids) have not hitherto been known as DHODH inhibitors. In a drug discovery process involving fragment and virtual screening, a number of fenamic acid derivatives have been discovered to be human DHODH inhibitors (unpublished data). One of the most potent compounds of this series is compound **7** (Table 1). Compound **7** was specifically designed to take advantage of two inhibitor-binding subsites, one of which is the "brequinar-like" binding site also called subsite 2, according to the classification of Baumgartner et al. (*28*), and which involves Gln47 and Arg136, and subsite 3, which involves Tyr356, Tyr147, and His56. Compound **7** is approximately as long as brequinar, but it lacks the bulky substituents in the ortho position of the benzoate ring (Table 1 and Figure 5). One notable difference in the conformation of this complex, compared to the complex with compound **6**, is that the side chain of Val134 is rotated toward the inhibitor (Figure 5). In the complex with compound **6**, this position of the side chain would have resulted in a steric clash with the Cl atom of the brequinar analogue. Not surprisingly, a similar conformation is adopted by Val134 in the inhibitor-free structure (Figure 3). The carboxylate group of compound **7** is rotated by approximately 30° compared to the position in compound **6**, which is probably required to optimize the interactions with Gln47 and Arg136. The side chains of both residues are shifted by approximately 0.5−1 Å toward the inhibitor and positioned 3.1 and 2.8 Å, respectively, from it (Figure 5). One of the unique features of compound **7** is a methoxy moiety in the meta position of the ring, which forms a hydrogen bond with the side chain of Tyr356 (2.6 Å). The distance to the side chain of the invariant His56 is also rather short (3.6 Å). The diphenyl ether moiety in compound **7** appears to be more flexible than in brequinar and is bent toward the opening of the pocket. This is presumably due

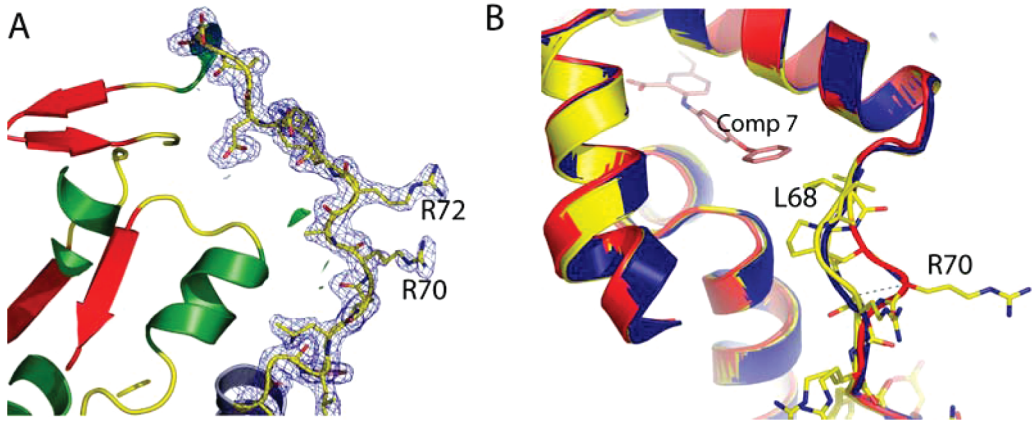

FIGURE 2: Loop connecting the N-terminal helical domain with the core catalytic domain. (A) A $3F_o - 2F_c$ electron density map (blue mesh) contoured at 1.2σ is superimposed on the model. Helices are colored green and strands red. Amino acid residues within the loop are shown as sticks, with nitrogens colored blue, oxygens red, and carbons yellow. (B) Superposition of the apo, compound **6**, and compound **7** complex structures showing changes in the conformation of the loop region around amino acid residues Leu68−Arg72 upon inhibitor binding (red, apo; yellow, compound **6** complex; blue, compound **7** complex).

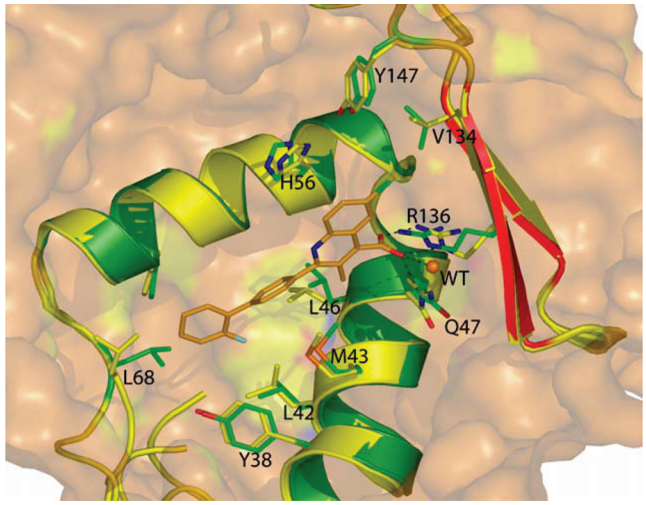

FIGURE 3: Binding of an inhibitor to DHODH and changes in side chain conformations in the inhibitor-binding pocket. The structures of the apoenzyme (green) and the complex with compound **6** (yellow) have been superimposed. Side chains and the inhibitor are shown as sticks. Compound **6** is colored light brown.

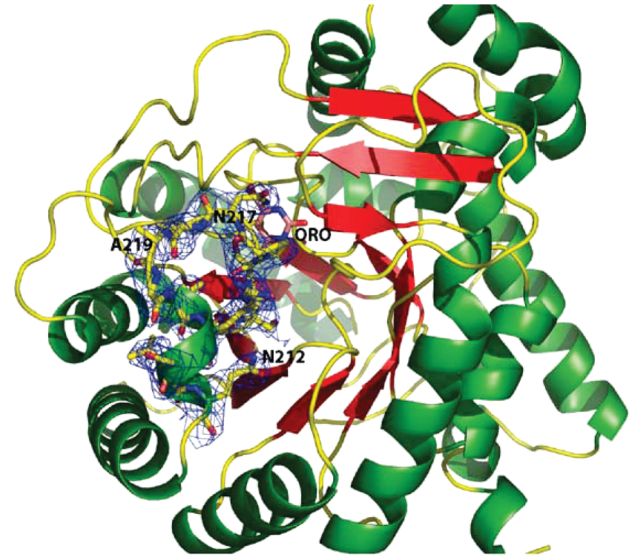

FIGURE 4: Loop covering the substrate binding site in apo-DHODH. A $3F_o - 2F_c$ electron density map (blue mesh) is shown superimposed on the loop region between residues Asn212 and Leu224. Amino acid side chains and the orotate are shown as sticks.

to the presence of "extra" atoms between the phenyl rings that are not present in the brequinar structure. Other small differences are observed in the conformations of the N-terminal residues and the loop region of Leu68−Arg72.

DISCUSSION

The low levels of amino acid sequence identity in the N-terminal domain of DHODH proteins from different organisms and the involvement of this region in inhibitor binding provide an opportunity for the design of new inhibitors with selectivities for particular organisms (*5, 30, 43, 44*). Some efforts have been made to develop analogues of brequinar and lefluonomide with higher potency, and also fewer and less adverse side effects (*18, 45–48*). The inhibitory activities of various compounds with structures similar to those of brequinar and redoxal, and with a novel chemotype, have also been analyzed using docking procedures and QSAR refinement (*49*). It was found that a large total van der Waals surface area and the presence of a negatively charged group in the compound are essential features of a good DHODH inhibitor. Compound **7**, which is a novel DHODH inhibitor, was designed according to these principles. It interacts with Gln47 and Arg136 (with a brequinar-like binding mode) and in addition with Tyr356 [subsites 2 and 3 as defined by Baumgartner et al. (*28*)]. This dual interaction with both subsites has only been observed previously in the complex with compound **5** (*34*). Compound **3** and some of its analogues are other examples of the compounds that interact with Tyr356 (*28*). However, compound **3** exhibited no observable interactions with Gln47 and Arg136, and it showed a binding that differs from the brequinar-like binding mode. In addition to the dual interaction mode, the structure of compound **7** has some specific features. Among these is the total length of the molecule, which causes the carboxylate-containing phenyl ring to position itself slightly more deeply inside the pocket, compared to compounds **1**, **5**, and **6**. This ensures more optimal interactions with Gln47 and Arg136. In addition, the methyl moiety in the methoxy group occupies a position similar to that of the Cl atom in **6** and the methyl group in **2**, which makes favorable hydrophobic interactions with

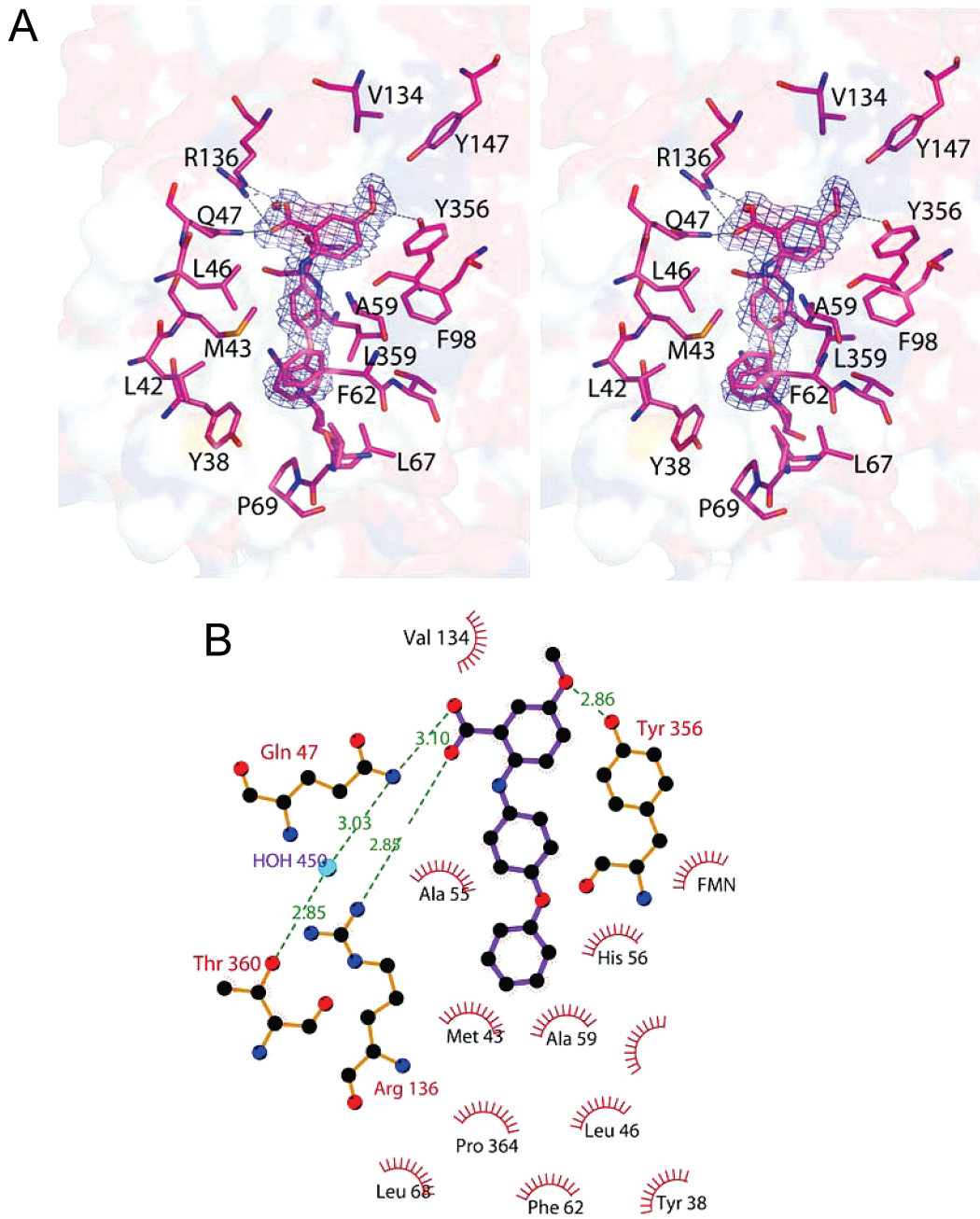

FIGURE 5: Compound **7** binding to human DHODH. (A) Stereoview showing the binding of compound **7** to DHODH. Dashed lines show hydrogen bonding interactions. An $F_o - F_c$ difference electron density map at 3σ is shown superimposed on the inhibitor structure. (B) Schematic plot of the interactions of compound **7** with DHODH. Dashed lines show hydrogen bonding interactions. The plot was prepared with Ligplot (*51*).

Val134 possible. It should be pointed out that we used a truncated form of human DHODH in our structural and activity studies. Previously, it has been observed that the N-terminal transmembrane part of DHODH had an impact on binding kinetics and potency for compounds **1** and **2** (*30, 33*). However, we did not observe any large variations in activity for compound **7** compared to kinetic studies with the full-length enzyme from mitochondrial membrane preparations of U973 cells (data not shown).

As seen in Table 1, compound **7** had a relatively lower affinity for human DHODH than compounds **1** and **4** did, which probably results from the higher flexibility of the diphenyl ether moiety positioned in the hydrophobic part of the binding tunnel. In compound **7**, this group is not optimally positioned: the last phenyl group points toward the opening of the tunnel and adopts a position similar to that of the CF_3 group in **2**. With these observations as a starting point, new compounds may be designed to take advantage of subsite 5 [as defined by Baumgartner et al. (*28*)], which would enable favorable interactions with the carbonyl oxygen of Leu67 and the hydroxyl group of Tyr38. In addition, interactions within the lipophilic pocket may be optimized. It should also be noted that the dynamic features seen in the complexes presented here suggest that the loops between Leu68 and Arg72 and between Asn212 and Leu224 have important regulatory roles in the activity of DHODH. Additional mutational studies should shed new light on the role(s) of these two loops.

ACKNOWLEDGMENT

We thank Lisbeth Witt for assay results, Stig Jönsson for synthesis of compound **6**, and others at Active Biotech Research for assistance during this work. We also thank the staff of the Max laboratory synchrotron for assistance during data collection.

REFERENCES

1. Fairbanks, L. D., Bofill, M., Ruckemann, K., and Simmonds, H. A. (1995) Importance of ribonucleotide availability to proliferating T-lymphocytes from healthy humans. Disproportionate expansion of pyrimidine pools and contrasting effects of de novo synthesis inhibitors. *J. Biol. Chem. 270*, 29682–29689.
2. Cutolo, M., Sulli, A., Ghiorzo, P., Pizzorni, C., Craviotto, C., and Villaggio, B. (2003) Anti-inflammatory effects of leflunomide on cultured synovial macrophages from patients with rheumatoid arthritis. *Ann. Rheum. Dis. 62*, 297–302.
3. Shawver, L. K., Schwartz, D. P., Mann, E., Chen, H., Tsai, J., Chu, L., Taylorson, L., Longhi, M., Meredith, S., Germain, L., Jacobs, J. S., Tang, C., Ullrich, A., Berens, M. E., Hersh, E., McMahon, G., Hirth, K. P., and Powell, T. J. (1997) Inhibition of platelet-derived growth factor-mediated signal transduction and tumor growth by N-[4-(trifluoromethyl)-phenyl]-5-methylisoxazole-4-carboxamide. *Clin. Cancer Res. 3*, 1167–1177.
4. Chen, S. F., Perrella, F. W., Behrens, D. L., and Papp, L. M. (1992) Inhibition of dihydroorotate dehydrogenase activity by brequinar sodium. *Cancer Res. 52*, 3521–3527.
5. Copeland, R. A., Marcinkeviciene, J., Haque, T. S., Kopcho, L. M., Jiang, W., Wang, K., Ecret, L. D., Sizemore, C., Amsler, K. A., Foster, L., Tadesse, S., Combs, A. P., Stern, A. M., Trainor, G. L., Slee, A., Rogers, M. J., and Hobbs, F. (2000) *Helicobacter pylori*-selective antibacterials based on inhibition of pyrimidine biosynthesis. *J. Biol. Chem. 275*, 33373–33378.
6. Herrmann, M. L., Schleyerbach, R., and Kirschbaum, B. J. (2000) Leflunomide: An immunomodulatory drug for the treatment of rheumatoid arthritis and other autoimmune diseases. *Immunopharmacology 47*, 273–289.
7. Liu, S., Neidhardt, E. A., Grossman, T. H., Ocain, T., and Clardy, J. (2000) Structures of human dihydroorotate dehydrogenase in complex with antiproliferative agents. *Structure 8*, 25–33.
8. Marcinkeviciene, J., Rogers, M. J., Kopcho, L., Jiang, W., Wang, K., Murphy, D. J., Lippy, J., Link, S., Chung, T. D., Hobbs, F., Haque, T., Trainor, G. L., Slee, A., Stern, A. M., and Copeland, R. A. (2000) Selective inhibition of bacterial dihydroorotate dehydrogenases by thiadiazolidinediones. *Biochem. Pharmacol. 60*, 339–342.
9. McRobert, L., and McConkey, G. A. (2002) RNA interference (RNAi) inhibits growth of *Plasmodium falciparum*. *Mol. Biochem. Parasitol. 119*, 273–278.
10. Burris, H. A., III, Raymond, E., Awada, A., Kuhn, J. G., O'Rourke, T. J., Brentzel, J., Lynch, W., King, S. Y., Brown, T. D., and von Hoff, D. D. (1998) Pharmacokinetic and phase I studies of brequinar (DUP 785; NSC 368390) in combination with cisplatin in patients with advanced malignancies. *Invest. New Drugs 16*, 19–27.
11. Chen, S. F., Papp, L. M., Ardecky, R. J., Rao, G. V., Hesson, D. P., Forbes, M., and Dexter, D. L. (1990) Structure-activity relationship of quinoline carboxylic acids. A new class of inhibitors of dihydroorotate dehydrogenase. *Biochem. Pharmacol. 40*, 709–714.
12. Cherwinski, H. M., Cohn, R. G., Cheung, P., Webster, D. J., Xu, Y. Z., Caulfield, J. P., Young, J. M., Nakano, G., and Ransom, J. T. (1995) The immunosuppressant leflunomide inhibits lymphocyte proliferation by inhibiting pyrimidine biosynthesis. *J. Pharmacol. Exp. Ther. 275*, 1043–1049.
13. Cherwinski, H. M., McCarley, D., Schatzman, R., Devens, B., and Ransom, J. T. (1995) The immunosuppressant leflunomide inhibits lymphocyte progression through cell cycle by a novel mechanism. *J. Pharmacol. Exp. Ther. 272*, 460–468.
14. Cramer, D. V. (1995) The use of xenografts for acute hepatic failure. *Transplant. Proc. 27*, 80–82.
15. Makowka, L., Sher, L. S., and Cramer, D. V. (1993) The development of Brequinar as an immunosuppressive drug for transplantation. *Immunol. Rev. 136*, 51–70.
16. Makowka, L., Chapman, F., and Cramer, D. V. (1993) Historical development of brequinar sodium as a new immunosuppressive drug for transplantation. *Transplant. Proc. 25*, 2–7.
17. Makowka, L., Tixier, D., Chaux, A., Hill, D., O'Neill, P., Eiras-Hreha, G., Wu, G. D., Cunneen, S., Cajulis, E., and Zajac, I. (1993) Use of brequinar sodium for preventing cardiac allograft rejection in primates. *Transplant. Proc. 25*, 48–53.
18. Pally, C., Smith, D., Jaffee, B., Magolda, R., Zehender, H., Dorobek, B., Donatsch, P., Papageorgiou, C., and Schuurman, H. J. (1998) Side effects of brequinar and brequinar analogues, in combination with cyclosporine, in the rat. *Toxicology 127*, 207–222.
19. Alldred, A., and Emery, P. (2001) Leflunomide: A novel DMARD for the treatment of rheumatoid arthritis. *Expert Opin. Pharmacother. 2*, 125–137.
20. Cohen, S., Cannon, G. W., Schiff, M., Weaver, A., Fox, R., Olsen, N., Furst, D., Sharp, J., Moreland, L., Caldwell, J., Kaine, J., and Strand, V. (2001) Two-year, blinded, randomized, controlled trial of treatment of active rheumatoid arthritis with leflunomide compared with methotrexate. Utilization of leflunomide in the treatment of rheumatoid arthritis trial investigator group. *Arthritis Rheum. 44*, 1984–1992.
21. Emery, P., Breedveld, F. C., Lemmel, E. M., Kaltwasser, J. P., Dawes, P. T., Gomor, B., Van Den, B. F., Nordstrom, D., Bjorneboe, O., Dahl, R., Horslev-Petersen, K., Rodriguez De La, S. A., Molloy, M., Tikly, M., Oed, C., Rosenburg, R., and Loew-Friedrich, I. (2000) A comparison of the efficacy and safety of leflunomide and methotrexate for the treatment of rheumatoid arthritis. *Rheumatology (Oxford, U.K.) 39*, 655–665.
22. Li, E. K., Tam, L. S., and Tomlinson, B. (2004) Leflunomide in the treatment of rheumatoid arthritis. *Clin. Ther. 26*, 447–459.
23. Shastri, V., Betkerur, J., Kushalappa, P. A., Savita, T. G., and Parthasarathi, G. (2006) Severe cutaneous adverse drug reaction to leflunomide: A report of five cases. *Indian J. Dermatol., Venereol., Leprol. 72*, 286–289.
24. Bjornberg, O., Rowland, P., Larsen, S., and Jensen, K. F. (1997) Active site of dihydroorotate dehydrogenase A from *Lactococcus lactis* investigated by chemical modification and mutagenesis. *Biochemistry 36*, 16197–16205.
25. Bjornberg, O., Gruner, A. C., Roepstorff, P., and Jensen, K. F. (1999) The activity of *Escherichia coli* dihydroorotate dehydrogenase is dependent on a conserved loop identified by sequence homology, mutagenesis, and limited proteolysis. *Biochemistry 38*, 2899–2908.
26. Hurt, D. E., Widom, J., and Clardy, J. (2006) Structure of *Plasmodium falciparum* dihydroorotate dehydrogenase with a bound inhibitor. *Acta Crystallogr. D62*, 312–323.
27. Norager, S., Jensen, K. F., Bjornberg, O., and Larsen, S. (2002) *E. coli* dihydroorotate dehydrogenase reveals structural and functional distinctions between different classes of dihydroorotate dehydrogenases. *Structure 10*, 1211–1223.
28. Baumgartner, R., Walloschek, M., Kralik, M., Gotschlich, A., Tasler, S., Mies, J., and Leban, J. (2006) Dual binding mode of a novel series of DHODH inhibitors. *J. Med. Chem. 49*, 1239–1247.
29. Hansen, M., Le, N. J., Johansson, E., Antal, T., Ullrich, A., Loffler, M., and Larsen, S. (2004) Inhibitor binding in a class 2 dihydroorotate dehydrogenase causes variations in the membrane-associated N-terminal domain. *Protein Sci. 13*, 1031–1042.
30. Knecht, W., and Loffler, M. (1998) Species-related inhibition of human and rat dihydroorotate dehydrogenase by immunosuppressive isoxazol and cinchoninic acid derivatives. *Biochem. Pharmacol. 56*, 1259–1264.
31. Knecht, W., Henseling, J., and Loffler, M. (2000) Kinetics of inhibition of human and rat dihydroorotate dehydrogenase by atovaquone, lawsone derivatives, brequinar sodium and polyporic acid. *Chem.-Biol. Interact. 124*, 61–76.
32. McLean, J. E., Neidhardt, E. A., Grossman, T. H., and Hedstrom, L. (2001) Multiple inhibitor analysis of the brequinar and leflunomide binding sites on human dihydroorotate dehydrogenase. *Biochemistry 40*, 2194–2200.
33. Ullrich, A., Knecht, W., Fries, M., and Loffler, M. (2001) Recombinant expression of N-terminal truncated mutants of the membrane bound mouse, rat and human flavoenzyme dihydroorotate dehydrogenase. A versatile tool to rate inhibitor effects. *Eur. J. Biochem. 268*, 1861–1868.
34. Hurt, D. E., Sutton, A. E., and Clardy, J. (2006) Brequinar derivatives and species-specific drug design for dihydroorotate dehydrogenase. *Bioorg. Med. Chem. Lett. 16*, 1610–1615.

35. Cerenius, Y., Stahl, K., Svensson, L. A., Ursby, T., Oskarsson, A., Albertsson, J., and Liljas, A. (2000) The crystallography beamline I711 at MAX II. *J. Synchrotron Radiat. 7*, 203–208.
36. Kabsch, W. (1993) Automatic Processing of Rotation Diffraction Data from Crystals of Initially Unknown Symmetry and Cell Constants. *J. Appl. Crystallogr. 26*, 795–800.
37. Brunger, A. T., Adams, P. D., Clore, G. M., Delano, W. L., Gros, P., Grosse-Kunstleve, R. W., Jiang, J. S., Kuszewski, J., Nilges, M., Pannu, N. S., Read, R. J., Rice, L. M., Simonson, T., and Warren, G. L. (1998) Crystallography & NMR system: A new software suite for macromolecular structure determination. *Acta Crystallogr. D54*, 905–921.
38. Jones, T. A., Zou, J. Y., Cowan, S. W., and Kjeldgaard, M. (1991) Improved Methods for Building Protein Models in Electron-Density Maps and the Location of Errors in These Models. *Acta Crystallogr. A47*, 110–119.
39. Murshudov, G. N., Vagin, A. A., and Dodson, E. J. (1997) Refinement of macromolecular structures by the maximum-likelihood method. *Acta Crystallogr. D53*, 240–255.
40. Hessen, D. P. (1987) 2-Phenyl-4quinolinecarboxylic acids and pharmaceutical compositions thereof. U.S. Patent 4,680,299.
41. Bruneau, J. M., Yea, C. M., Spinella-Jaegle, S., Fudali, C., Woodward, K., Robson, P. A., Sautes, C., Westwood, R., Kuo, E. A., Williamson, R. A., and Ruuth, E. (1998) Purification of human dihydro-orotate dehydrogenase and its inhibition by A77 1726, the active metabolite of leflunomide. *Biochem. J. 336* (Part 2), 299–303.
42. Cleaveland, E. S., Monks, A., Vaigro-Wolff, A., Zaharevitz, D. W., Paull, K., Ardalan, K., Cooney, D. A., and Ford, H., Jr. (1995) Site of action of two novel pyrimidine biosynthesis inhibitors accurately predicted by the compare program. *Biochem. Pharmacol. 49*, 947–954.
43. Baldwin, J., Farajallah, A. M., Malmquist, N. A., Rathod, P. K., and Phillips, M. A. (2002) Malarial dihydroorotate dehydrogenase. Substrate and inhibitor specificity. *J. Biol. Chem. 277*, 41827–41834.
44. Ullrich, A., Knecht, W., Piskur, J., and Loffler, M. (2002) Plant dihydroorotate dehydrogenase differs significantly in substrate specificity and inhibition from the animal enzymes. *FEBS Lett. 529*, 346–350.
45. Bertolini, G., Aquino, M., Biffi, M., d'Atri, G., Di, P. F., Ferrario, F., Mascagni, P., Somenzi, F., Zaliani, A., and Leoni, F. (1997) A new rational hypothesis for the pharmacophore of the active metabolite of leflunomide, a potent immunosuppressive drug. *J. Med. Chem. 40*, 2011–2016.
46. Huang, W. H., Yang, C. L., Lee, A. R., and Chiu, H. F. (2003) Leflunomide analogues as potential antiinflammatory agents. *Chem. Pharm. Bull. 51*, 313–314.
47. Schuurman, H. J., Tanner, M., Pally, C., and Jaffee, B. D. (1998) Brequinar and brequinar analogues in rat allo- and xenotransplantation. *Transplant. Proc. 30*, 2240–2243.
48. Silva Junior, H. T., and Morris, R. E. (1997) Leflunomide and malononitrilamides. *Am. J. Med. Sci. 313*, 289–301.
49. Leban, J., Saeb, W., Garcia, G., Baumgartner, R., and Kramer, B. (2004) Discovery of a novel series of DHODH inhibitors by a docking procedure and QSAR refinement. *Bioorg. Med. Chem. Lett. 14*, 55–58.
50. DeLano, W. L. (2002) *The PyMOL Molecular Graphics System*, DeLano Scientific, San Carlos, CA.
51. Wallace, A. C., Laskowski, R. A., and Thornton, J. M. (1995) LIGPLOT: A program to generate schematic diagrams of protein-ligand interactions. *Protein Eng. 8*, 127–134.

BI8003318